Measurement of 3-D position and orientation of rigid bodies using a 3-facet mirror

W. S. Park [a], H. S. Cho [a], Y. K. Byun [b], N. Y. Park [b], and D. K. Jung [b]

[a] Department of Mechanical Engineering, Korea Advanced Institute of Science and Technology
[b] Samsung Advanced Institute of Technology

ABSTRACT

In this paper, a new measuring system is proposed which can measure the 3-dimensional position and orientation of rigid bodies. Its measurement principle is based on detection of laser beam reflected from a specially fabricated mirror that looks like a triangular pyramid having an equilateral cross-sectional shape. The mirror has three lateral reflective surfaces inclined 45° to its bottom surface. We call this mirror 3-facet mirror. The 3-facet mirror is mounted on the object whose position and orientation are to be measured. The measurement is operated by a laser-based optical system composed of a 3-facet mirror, a He-Ne laser source, three position-sensitive detectors(PSD). In the sensor system, three PSDs are located at three corner points of a triangular formation, which is an equilateral triangular formation lying parallel to the reference plane. The sensitive areas of three PSDs are oriented toward the center point of the triangular formation. The object whose position and orientation are to be measured is situated at the center with the 3-facet mirror on its top surface. A laser beam is emitted from the He-Ne laser source located at the upright position and vertically incident on the top of the 3-facet mirror. Since each reflective facet faces toward each PSD, the laser beam is reflected at the 3-facet mirror and splits into three sub-beams, each of which is reflected from the three facets and finally arrives at three PSDs, respectively. Since each PSD is a 2-dimensional sensor, we can acquire the information on the 6-degree-of-freedom motion of the 3-facet mirror. From this principle, we can get the 3-dimensional position and orientation of any object simply by mounting the 3-facet mirror on the object. In this paper, we model the relationship between the 3-dimensional position and orientation of the object and the outputs of three PSDs. And, a series of experiments are performed to demonstrate the effectiveness and accuracy of the proposed method. The experimental results show that the proposed sensing system can be an effective means of obtaining 3-dimensional position and orientation of arbitrary objects. The resolution of the experimental system is found to be approximately two micrometers in translation and five micro-radians in rotation. By virtue of the easiness in application, the measurement principle can be applied to a wide range of applications such as 3-D fine motion of robotic manipulators, machining tools, sliders flying on magnetic disks of HDDs, positioning stages, etc.

Keywords: 3-dimensional pose, 6-DOF motion, 3-facet mirror, optical metrology, position-sensitive detector

1. INTRODUCTION

A rigid body, which is not constrained to any kinematic condition, has six degrees of kinematic freedom in space. Therefore, it needs six spatial parameters such as x, y, z in translation and roll, pitch, yaw in rotation to fully describe the 3-dimensional position and orientation of a rigid body. In order to simultaneously measure the 3-dimensional position and orientation of rigid bodies, a lot of approaches are proposed such as computer vision, 6-DOF master devices in master-slave mechanisms, inertial navigation system(INS) comprises of a tri-axial accelerometer along with three gyros, etc.

Computer vision technologies[1-3], most of which use camera images, are widely used for recognizing 3-dimensional position and orientation of rigid bodies since they are effective and easily implemented. Many of computer vision approaches use landmarks that are designed so that we can extract their features easily and accurately. These approaches can be effective means to locate mobile robots, to estimate the position and orientation of end-effectors of robot manipulators, etc. However, they are hardly applied to precise measurements. The precision of computer vision approaches is limited to the order of few millimeters or hundreds of micrometers.

[a] Prof. H. S. Cho (correspondence): E-mail: hscho@lca.kaist.ac.kr; WWW: http://lca.kaist.ac.kr; Tel: +82-42-869-3213; Fax: +82-42-869-3210

We can see another 6-DOF sensor in master-slave mechanisms[4-6] that are widely used in tele-operation and virtual reality systems. In such systems, the kinematic parameters of master devices are identified and six encoders, either optical or magnetic types, measure the joint coordinate of each link. Through the forward kinematics of the master device, we can estimate the 3-dimensional position and orientation of the end-effector. Thus, master mechanisms are a kind of 6-DOF sensor. The order of precision of the master mechanisms is similar to that of computer vision sensors, few millimeters or hundreds of micrometers.

Six degrees of freedom motion of aircraft, missiles, and rockets are estimated by inertial navigation systems(INS)[7-9]. INS measures linear and angular accelerations in 6-DOF and integrates them with respect to time to estimate the 3-dimensional position, x, y, and z-coordinates, and rotation, roll, pitch, and yaw-angles. These approaches needs no landmark as used in computer vision approaches and quite accurate for a while after initiation of integration. But errors in all of six components are accumulated and keep increasing as time goes. The accumulated errors are hardly bound to some limit values. Thus these approaches are not proper to precise measurement either.

For precise measurement of position and rotation in the order of micrometers and micro-radians respectively, optical instruments such as laser interferometer and laser doppler vibrometer are widely used[10-12]. These instruments show very high precision even in the order of nanometers in translation. These sensors are basically for one-dimensional measurement. For higher dimensional measurement such as two or three dimensional position plus rotation, it needs to integrate several laser interferometers and laser doppler vibrometers, which is a very difficult task and actually impossible for 6-DOF applications.

In this paper, a new measuring system is proposed which can measure the 3-dimensional position and orientation of rigid bodies in the precision order of micrometers and micro-radians. For precise measurement, we utilize a laser source, a specially fabricated mirror, and three position-sensitive detectors(PSD). The specially fabricated mirror looks like a triangular pyramid having an equilateral cross-sectional shape, we call this mirror 3-facet mirror. Three PSDs are located at three corner points of a triangular formation, which is an equilateral triangular formation lying parallel to the reference plane. A laser beam is emitted from the He-Ne laser source located at the upright position and vertically incident on the top of the 3-facet mirror. The laser beam is reflected at the 3-facet mirror and splits into three sub-beams, each of which is reflected from the three facets and finally arrives at three PSDs, respectively. From the signals of the PSDs, we can calculate the 3-dimensional position and orientation of the 3-facet mirror, and we can get the 3-dimensional position and orientation of any object simply by mounting the 3-facet mirror on the object. In this paper, we model the relationship between the 3-dimensional position and orientation of the object and the outputs of three PSDs. And, a series of experiments are performed to demonstrate the effectiveness and accuracy of the proposed method. The experimental results show that the proposed sensing system can be an effective means of obtaining 3-dimensional position and orientation of arbitrary objects.

2. PRINCIPLE OF SENSOR SYSTEM

2.1 System configuration

Figure 1 shows the overall configuration of the sensor system that we proposed for precise measurement of 3-dimensional position and orientation of objects. As shown in the figure, the sensor system is composed of a mirror of pyramidal shape, a He-Ne laser source, three position-sensitive detectors(PSD). In the figure, the laser beam is emitted from the He-Ne laser source located at the upright position and vertically incident on the top of a mirror of pyramid shape. The mirror is specially fabricated, which has an equilateral triangular cross-section as shown in Figure 2. We call this mirror 3-facet mirror since the mirror has three lateral reflective surfaces inclined 45° to its bottom surface. As shown in Figure 2, the laser beam is reflected at the 3-facet mirror and splits into three sub-beams.

As shown in Figure 1, three PSDs are located at three corner points of a triangular formation, which is an equilateral triangular formation lying parallel to the reference plane. The sensitive areas of three PSDs are oriented toward the center point of the triangular formation. The object whose position and orientation are to be measured is situated at the center with the 3-facet mirror on its top surface. Each reflective facet of the 3-facet mirror faces toward each PSD and the three laser beams reflected at the 3-facet mirror arrive at three PSDs, respectively. Since each PSD is a 2-dimensional sensor, we can acquire the information on the 6-degree-of-freedom motion of the 3-facet mirror. If we mount the 3-facet mirror on any object, then we can also measure the 6-degree-of-freedom motion of the object. The mathematical relationship between the

3-dimensional pose of the 3-facet mirror and the six outputs of the PSDs is to be explained in next section.

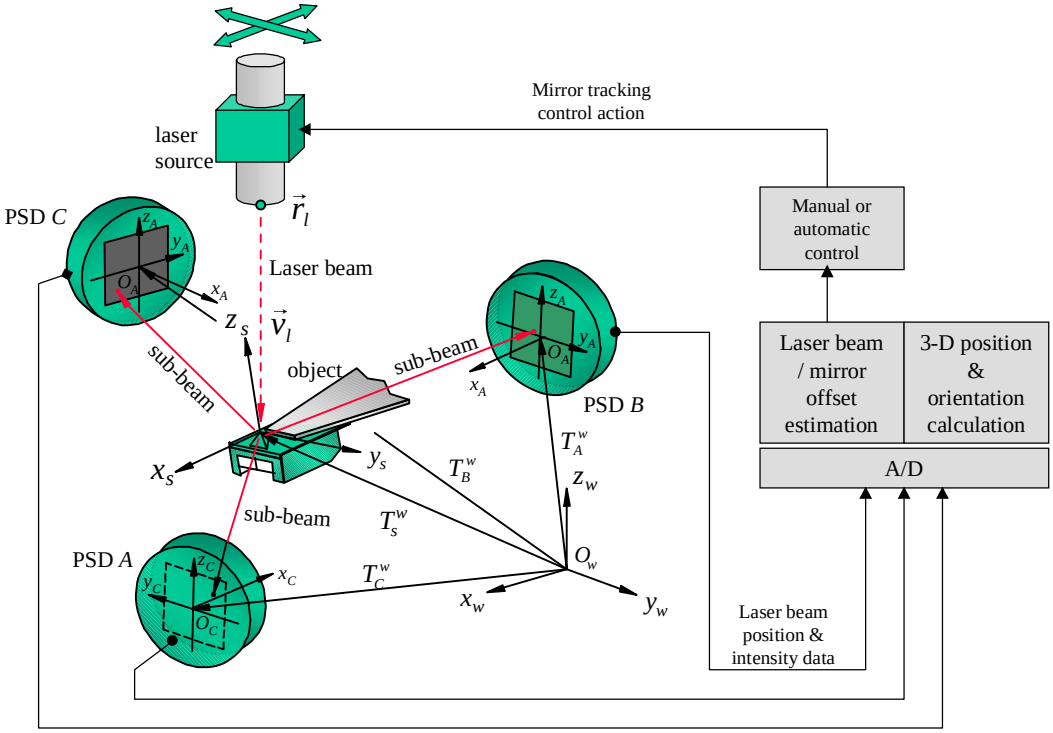

Figure 1 System configuration

In Figure 1, each PSD gives us the 2-dimensional position of laser beam spot and its intensity. Thus, three PSDs give us totally six outputs related with the positions of the laser beam spots and three intensity data. Thus, for acquiring whole data, it needs an analog-to-digital(A/D) conversion board with at least nine channels. We can calculate the x, y, z translation and roll, pitch, yaw rotation from the six positional data through the sensor model to be presented in next section.

In the measurement system, the laser beam should illuminates the top of the 3-facet mirror. Thus, it needs to control the position of laser beam to meet the top of the 3-facet mirror. The three intensity data are used to control the laser beam position so that the beam center always meets the top of the 3-facet mirror. We can see the laser beam from the laser source splits into three sub-beams so that each sub-beam shares the light power with each other. If the center of the original laser beam exactly meets the top of the 3-facet mirror, the light powers of the three sub-beams are exactly equal. From this principle, we can control the position of the laser beam through comparing the intensity signals of three PSDs with each others.

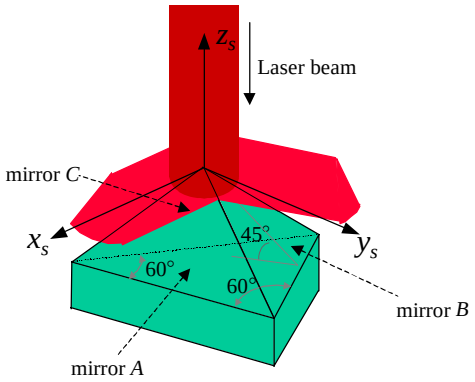

Figure 2 3-facet mirror reflecting a laser beam into three beams

2.2 Sensor model

To model the relationship between the 3-dimensional pose of the 3-facet mirror and the six positional signals of three PSDs, we perform a series of ray tracing as follows.

At first, we model the original laser beam on a straight line starting from a point, the laser source, whose direction vector is $\vec{v}_l$ and the position of source point is $\vec{r}_l$. As described above, the direction of laser beam is kept to be vertical and the position is controlled so that its center meets the top of the 3-facet mirror. Therefore the direction vector of the laser beam is constant as

$$\vec{v}_l = [0 \quad 0 \quad -1]^T \tag{1}$$

but the position is variable.

Secondly, the three sub-beams are calculated through the light reflection law after the geometrical models of three mirror surfaces are obtained. The mirror surfaces are modeled as 3-dimensional plane. As shown in Figure 2, the three mirror planes are modeled with respect to the reference frame, o_s, which is located at the top of the 3-facet mirror. The *z*-axis of o_s is vertical to the bottom surface of the 3-facet mirror and the *x*-axis is vertical to a bottom edge. We call the mirror, that faces in the direction of x-axis, mirror A, and the others mirror B and C. The equations of planes of the three mirrors are

$$\begin{aligned}
&\textit{Mirror } A: && \frac{1}{\sqrt{2}}x_s + \frac{1}{\sqrt{2}}z_s = 0 \\
&\textit{Mirror } B: && -\frac{1}{2\sqrt{2}}x_s + \frac{\sqrt{3}}{2\sqrt{2}}y_s + \frac{1}{\sqrt{2}}z_s = 0 \\
&\textit{Mirror } C: && -\frac{1}{2\sqrt{2}}x_s - \frac{\sqrt{3}}{2\sqrt{2}}y_s + \frac{1}{\sqrt{2}}z_s = 0.
\end{aligned} \tag{2}$$

And they can be modeled with respect to the world coordinate system, o_w. The equations of the mirrors A, B, and C are expressed with the position and orientation of the 3-facet mirror. The position and orientation of the 3-facet mirror include x, y, z translations and roll, pitch, yaw rotations, which are expressed as a homogeneous transform matrix[13], T_s^w, in Figure 1. The components of T_s^w are

$$T_s^w = \begin{bmatrix} c\alpha c\beta & c\alpha s\beta s\gamma - s\alpha c\gamma & c\alpha s\beta c\gamma + s\alpha s\gamma & t_x \\ s\alpha c\beta & s\alpha s\beta s\gamma + c\alpha c\gamma & s\alpha s\beta c\gamma - c\alpha s\gamma & t_y \\ -s\beta & c\beta s\gamma & c\beta c\gamma & t_z \\ 0 & 0 & 0 & 1 \end{bmatrix} \tag{3}$$

where α, β, and γ are the angles of roll, pitch, and yaw rotations, and t_x, t_y, and t_z are the translations in x_w, y_w, and z_w directions, respectively, and where $c\alpha$, $s\alpha$, and $c\beta$ represent $\cos\alpha$, $\sin\alpha$, and $\cos\beta$, and so on. Through this transform, we get the equations of mirrors *A*, *B*, and *C* represented with respect to the world coordinate systems, x_w, y_w, and z_w, as

$$\begin{aligned}
&l_A(x_w - t_x) + m_A(y_w - t_y) + n_A(z_w - t_z) = 0 \\
&l_B(x_w - t_x) + m_B(y_w - t_y) + n_B(z_w - t_z) = 0 \\
&l_C(x_w - t_x) + m_C(y_w - t_y) + n_C(z_w - t_z) = 0
\end{aligned} \tag{4}$$

where,

$$
\begin{aligned}
l_A &= \frac{1}{\sqrt{2}}(c\alpha c\beta + c\alpha s\beta c\gamma + s\alpha s\gamma) \\
m_A &= \frac{1}{\sqrt{2}}(s\alpha c\beta + s\alpha s\beta c\gamma - c\alpha s\gamma) \\
n_A &= -\frac{1}{\sqrt{2}}(s\beta + c\beta c\gamma)
\end{aligned} \tag{5}
$$

$$
\begin{aligned}
l_B &= -\frac{1}{2\sqrt{2}}c\alpha c\beta + \frac{\sqrt{3}}{2\sqrt{2}}(c\alpha s\beta s\gamma - s\alpha s\gamma) + \frac{1}{\sqrt{2}}(c\alpha s\beta c\gamma + s\alpha s\gamma) \\
m_B &= -\frac{1}{2\sqrt{2}}s\alpha c\beta + \frac{\sqrt{3}}{2\sqrt{2}}(s\alpha s\beta s\gamma + c\alpha c\gamma) + \frac{1}{\sqrt{2}}(s\alpha s\beta c\gamma - c\alpha s\gamma) \\
n_B &= \frac{1}{2\sqrt{2}}s\beta + \frac{\sqrt{3}}{2\sqrt{2}}c\beta s\gamma + \frac{1}{\sqrt{2}}c\beta c\gamma
\end{aligned} \tag{6}
$$

$$
\begin{aligned}
l_C &= -\frac{1}{2\sqrt{2}}c\alpha c\beta - \frac{\sqrt{3}}{2\sqrt{2}}(c\alpha s\beta s\gamma - s\alpha s\gamma) + \frac{1}{\sqrt{2}}(c\alpha s\beta c\gamma + s\alpha s\gamma) \\
m_C &= -\frac{1}{2\sqrt{2}}s\alpha c\beta - \frac{\sqrt{3}}{2\sqrt{2}}(s\alpha s\beta s\gamma + c\alpha c\gamma) + \frac{1}{\sqrt{2}}(s\alpha s\beta c\gamma - c\alpha s\gamma) \\
n_C &= \frac{1}{2\sqrt{2}}s\beta - \frac{\sqrt{3}}{2\sqrt{2}}c\beta s\gamma + \frac{1}{\sqrt{2}}c\beta c\gamma
\end{aligned} \tag{7}
$$

From the above equations, we can get the direction vectors of the three sub-beams using light reflection law[14] as

$$
\begin{aligned}
\vec{v}_A &= [v_{Ax} \quad v_{Ay} \quad v_{Az}]^T = M_A\vec{v}_l \\
\vec{v}_B &= [v_{Bx} \quad v_{By} \quad v_{Bz}]^T = M_B\vec{v}_l \\
\vec{v}_C &= [v_{Cx} \quad v_{Cy} \quad v_{Cz}]^T = M_C\vec{v}_l
\end{aligned} \tag{8}
$$

where the reflection matrices of the three mirror surfaces are

$$
\begin{aligned}
\mathbf{M}_A &= \begin{bmatrix} 1-2l_A^2 & -2l_Am_A & -2l_An_A \\ -2l_Am_A & 1-2m_A^2 & -2n_Am_A \\ -2l_An_A & -2n_Am_A & 1-2n_A^2 \end{bmatrix} \\
\mathbf{M}_B &= \begin{bmatrix} 1-2l_B^2 & -2l_Bm_B & -2l_Bn_B \\ -2l_Bm_B & 1-2m_B^2 & -2n_Bm_B \\ -2l_Bn_B & -2n_Bm_B & 1-2n_B^2 \end{bmatrix} \\
\mathbf{M}_C &= \begin{bmatrix} 1-2l_C^2 & -2l_Cm_C & -2l_Cn_C \\ -2l_Cm_C & 1-2m_C^2 & -2n_Cm_C \\ -2l_Cn_C & -2n_Cm_C & 1-2n_C^2 \end{bmatrix}
\end{aligned} \tag{9}
$$

By now, we get the models of the three sub-beams in the forms of mathematical equations of lines as

$$\begin{aligned}
\frac{x_w - t_x}{v_{Ax}} &= \frac{y_w - t_y}{v_{Ay}} = \frac{z_w - t_z}{v_{Az}} \\
\frac{x_w - t_x}{v_{Bx}} &= \frac{y_w - t_y}{v_{By}} = \frac{z_w - t_z}{v_{Bz}} \\
\frac{x_w - t_x}{v_{Cx}} &= \frac{y_w - t_y}{v_{Cy}} = \frac{z_w - t_z}{v_{Cz}}
\end{aligned} \tag{10}$$

respectively. These three sub-beams go incident on the three PSDs, respectively, as shown in Figure 1. The final output of the system model is the six positional outputs of the three PSDs. The positional ouputs are the coordinates of the laser beam spot on the PSDs. Thus, it needs to calculate the coordinates of intersections between the above lines and the planes of the sensitive areas of PSDs. To perform this task, it needs to describe the geometrical configuration of PSDs, which is shown in Figure 3. In the figure, the 3-facet mirror is in case of being located at the origin of the reference frame, o_w. Three PSDs are equally far from the origin of o_w, one of which, PSD *A*, is located on the *x*-axis of o_w, and the others are located on the lines that make angles of 120° to the x_w axis. The frames, o_A, o_B, and o_C, are located at the centers of the PSDs, PSD A, PSD B, and PSD C, respectively, whose *x*-axes are directed toward the system origin, o_w.

The six positional outputs of the PSDs are three couples of coordinates, each of which is the 2-dimensional coordinates of a laser beam spot on a PSD's surface with respect to each coordinate frame. In Figure 3, the coordinates of the laser beam spots can be obtained through calculating the geometrical intersection points between the laser beams and the PSD surfaces. In the figure, we can see the three PSDs are equally far from the system origin, o_w. The radial distance is represented as R_{PSD}. And the surface normals of the three PSDs are make angles of 120° to each other.

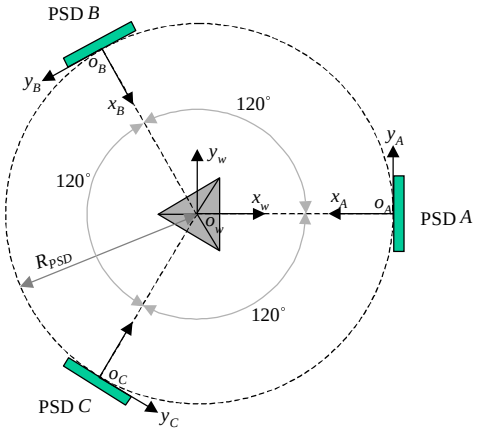

Figure 3 Layout and coordinate systems of the PSDs

To obtain the intersection points, each model of the laser beam is transformed with respect to each PSD coordinate frame. To do so, the homogeneous transform matrices that describe the positions and orientations of the PSDs should be prepared as follows.

$$T_A^w = \begin{bmatrix} -1 & 0 & 0 & R_{PSD} \\ 0 & -1 & 0 & 0 \\ 0 & 0 & 1 & 0 \\ 0 & 0 & 0 & 1 \end{bmatrix}, \quad T_B^w = \begin{bmatrix} \frac{1}{2} & \frac{\sqrt{3}}{2} & 0 & -\frac{R_{PSD}}{2} \\ -\frac{\sqrt{3}}{2} & \frac{1}{2} & 0 & \frac{\sqrt{3}}{2}R_{PSD} \\ 0 & 0 & 1 & 0 \\ 0 & 0 & 0 & 1 \end{bmatrix}, \quad T_B^w = \begin{bmatrix} \frac{1}{2} & -\frac{\sqrt{3}}{2} & 0 & -\frac{R_{PSD}}{2} \\ \frac{\sqrt{3}}{2} & \frac{1}{2} & 0 & -\frac{\sqrt{3}}{2}R_{PSD} \\ 0 & 0 & 1 & 0 \\ 0 & 0 & 0 & 1 \end{bmatrix} \tag{11}$$

Through these homogeneous transforms, we can get the new equations of the three laser beams with respect to the PSDs' coordinate systems respectively as

$$\begin{aligned}
&\frac{x_A + t_x - R_{PSD}}{v_{Ax}} = \frac{y_A + t_y}{v_{Ay}} = -\frac{z_A - t_z}{v_{Az}} \\
&\frac{x_B - t_x - \sqrt{3}t_y + R_{PSD}}{v_{Bx} + \sqrt{3}v_{By}} = \frac{y_B + \sqrt{3}t_x - t_y - \sqrt{3}R_{PSD}}{-\sqrt{3}v_{Bx} + v_{By}} = \frac{z_B - t_z}{v_{Bz}} \\
&\frac{x_C - t_x + \sqrt{3}t_y + R_{PSD}}{v_{Cx} - \sqrt{3}v_{Cy}} = \frac{y_C - \sqrt{3}t_x - t_y + \sqrt{3}R_{PSD}}{\sqrt{3}v_{Cx} + v_{Cy}} = \frac{z_C - t_z}{v_{Cz}}
\end{aligned} \tag{12}$$

To obtain the laser beam spots on the PSDs, we calculate the geometrical intersection points between the line equations in Eqs.(12) and the plane equations of PSD surfaces. As shown in Figure 3, the surfaces of the three PSDs can be expressed as similar plane equations as

$$\begin{aligned}
x_A &= 0 \\
x_B &= 0 \\
x_C &= 0
\end{aligned} \tag{13}$$

Substituting the above plane equations, Eqs.(13), to Eqs.(12), and rearranging y_A and z_A, i.e. the 2-dimensional coordinates of the laser beam spot on PSD *A* are obtained as

$$\begin{aligned}
u_A &= y_A\big|_{x_A=0} = \frac{v_{Ay}t_x - v_{Ax}t_y - v_{Ay}R_{PSD}}{v_{Ax}} \\
v_A &= z_A\big|_{x_A=0} = \frac{-v_{Az}t_x + v_{Ax}t_z + v_{Az}R_{PSD}}{v_{Ax}}
\end{aligned} \tag{14}$$

and similarly for PSD *B* and PSD *C*, the following equations give us the coordinates of the laser beams as follows.

$$\begin{aligned}
u_B &= y_B\big|_{x_B=0} = \frac{-\sqrt{3}v_{Bx} + v_{By}}{v_{Bx} + \sqrt{3}v_{By}}(-t_x - \sqrt{3}t_y + R_{PSD}) - \sqrt{3}t_x + t_y + \sqrt{3}R_{PSD} \\
v_B &= z_B\big|_{x_B=0} = \frac{v_{Bz}}{v_{Bx} + \sqrt{3}v_{By}}(-t_x - \sqrt{3}t_y + R_{PSD}) + t_z
\end{aligned} \tag{15}$$

$$\begin{aligned}
u_C &= y_C\big|_{x_C=0} = \frac{\sqrt{3}v_{Cx} + v_{Cy}}{v_{Cx} - \sqrt{3}v_{Cy}}(-t_x + \sqrt{3}t_y + R_{PSD}) + \sqrt{3}t_x + t_y - \sqrt{3}R_{PSD} \\
v_C &= z_C\big|_{x_C=0} = \frac{v_{Cz}}{v_{Cx} - \sqrt{3}v_{Cy}}(-t_x + \sqrt{3}t_y + R_{PSD}) + t_z
\end{aligned} \tag{16}$$

Here, (u_A, v_A), (u_B, v_B), and (u_C, v_C) are the three couples of 2-dimensional coordinates of the three laser beam spots on PSD A, B, and C, respectively.

By now, we have modeled the relationship between the 3-dimensional pose, i.e. t_x, t_y, t_z, γ, β, and α, and the three couples of 2-dimensional coordinates of the three laser beam spots on PSD A, B, and C, (u_A, v_A), (u_B, v_B), and (u_C, v_C). Through Eqs. (1) ~ (16), we can calculate (u_A, v_A), (u_B, v_B), and (u_C, v_C) with given t_x, t_y, t_z, γ, β, and α. When we perform actual measurement with the proposed sensor system, we have to perform the inversion of above sequences of

calculation, i.e. calculation of t_x, t_y, t_z, γ, β, and α with given (u_A, v_A), (u_B, v_B), and (u_C, v_C). This is performed through a numerical way, Newton's method[15], through which we have successfully got the solution, t_x, t_y, t_z, γ, β, and α, with given (u_A, v_A), (u_B, v_B), and (u_C, v_C), in the experiments to be presented next section.

3. EXPERIMENTS

In order to verify the principle and the effectiveness of the proposed measurement method, we have implemented an experimental system and performed a series of experiments. Figure 4 shows the experimental system that we implemented. In the figure, the laser beam is artificially represented as straight lines, which is not shown in actual situation. The configuration of the experimental system is similar to the one explained in the previous section, but has two additional instruments such as interferometer and 6-axis stage. The interferometer is used for benchmarking the proposed sensor system and the 6-axis stage is used for actuating the 3-facet mirror with high precision.

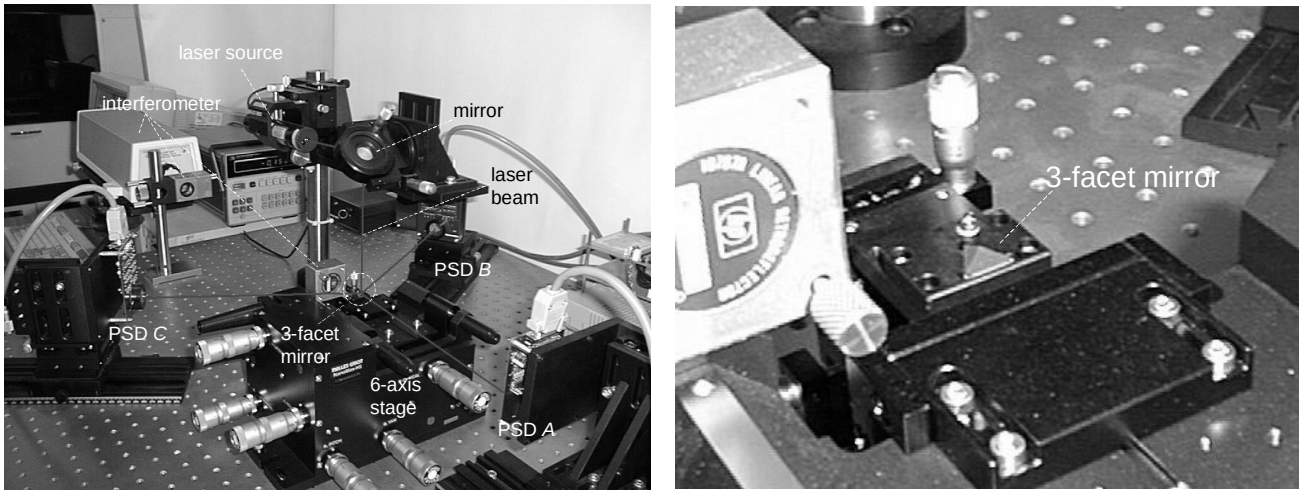

(a) (b)

Figure 4 Photograph of experimental system: (a) Whole system; (b) 3-facet mirror

The experiments include six sets of benchmarking each axis. A set of benchmarking a single axis includes a series of comparisons between the readings of the proposed sensor and the interferometer readings. Figure 4(a) shows the situation of benchmarking the x_w-readings of the proposed sensor. The interferometer is aligned so that it can measure the x_w-movement. The 3-facet mirror is sequentially positioned and moved in the x_w-direction while the series of both readings are compared with each other. The movement is performed through actuating the x-axis actuator of the 6-axis stage. The actuators of the 6-axis stage are actuated by manual operation. For other axes such as y_w-translation, z_w-translation, rolling, pitching, and yawing, similar tasks are performed, but the configuration of the interferometer is changed to measure the relevant axis movement. The main parameters of the experimental system and the specifications of its components are listed in Table 1.

Figure 5 ~ Figure 10 show the experimental results. In the left side of the figures, the measured displacements, both positional and rotational, are plotted with respect to the reference values, i.e. the interferometer readings. And the right side of the figures, the errors between the measured values and the interferometer readings are plotted with respect to the interferometer readings. On each point in the figures, data have been acquired fifty times, whose mean values are connected in solid lines. And the minimum and maximum value as well as the standard deviation are plotted on each point of measurement. The upper and lower positions of standard deviation are represented as "+sigma" and "-sigma" respectively.

In Figure 5 ~ Figure 7, we can see the measurement precision of the proposed sensor in case of linear translation. As shown in the figures, the ranges of the translations are very small. For x_w-translation, the position intervals of the data points are equally given as 1.44 μm, and for other directions such as y_w and z_w-translations, the intervals are 1.42 and 0.93 μm, respectively. This is in order that we may see the precision limits of the proposed sensor. The solid lines in the left side figures, which represent mean values of the sensor readings, do not look straight but crooked since the measurement ranges are too small so that random noises are relatively large. In other words, the measurement conditions such as ranges and

intervals are near to the sensor's precision limits. The relative uncertainties in Table 2, which are larger than 10%, reveal this fact. If the measurement ranges are chosen as sufficiently large, the solid lines get straight, which can be done simply by adopting PSDs of large sensitive areas. In the experimental system configured in this paper, has three PSDs having sensitive areas of 13 mm x 13 mm. This size can give us so large measurement ranges of at least 10 mm when a single axis of translation is under measurement.

Table 1 Specifications of the experimental system

Components	Specifications		
He-Ne Laser	Power		0.8 mW
	Beam diameter		0.46 mm
	Beam orientation at 3-facet mirror		Vertical (const.)
3-facet mirror	Azimuth of surface normal		45°
	Longitudinal distance between surface normals		120°
	Surface flatness		λ/10 at 632.8 nm
PSD	Size of sensitive area		13 mm x 13 mm
	Layout	Radial distance from the system origin	250 mm
		Longitudinal distance between PSDs	120°
		Orientations	See Figure 3
Laser interferometer	Relative uncertainty		10^{-6}
	Resolution	Linear	10 nm
		Angular	0.1 arcsec
6-axis stage	Travel range	Linear	4 mm
		Angular	6°
	Resolution	Linear	1 μm
		Angular	4 arcsec

In Figure 8 ~ Figure 10, we can see the measurement results for *rolling*, *pitching*, and *yawing* movements. As shown in the figures, the solid lines, which represent the means of the sensor readings, look straight while those of translation measurements are crooked. In the rotation measurements such as rolling, pitching, and yawing, the angular intervals are given as 15.5 μrad, 15.5 μrad, and 16.3 μrad for *rolling*, *pitching*, and *yawing*, respectively. From this, the proposed sensor can easily measure those fine rotations, i.e. the rotation intervals. As shown in Table 2, the relative uncertainties are smaller than those of translation measurements. The measurement precision of the proposed sensor for rotation is linearly proportional to the radial distance of PSDs from the system origin, o_w. If the distance gets two times then the precision of rotation measurement is improved by two times, but measurement range reduces by half.

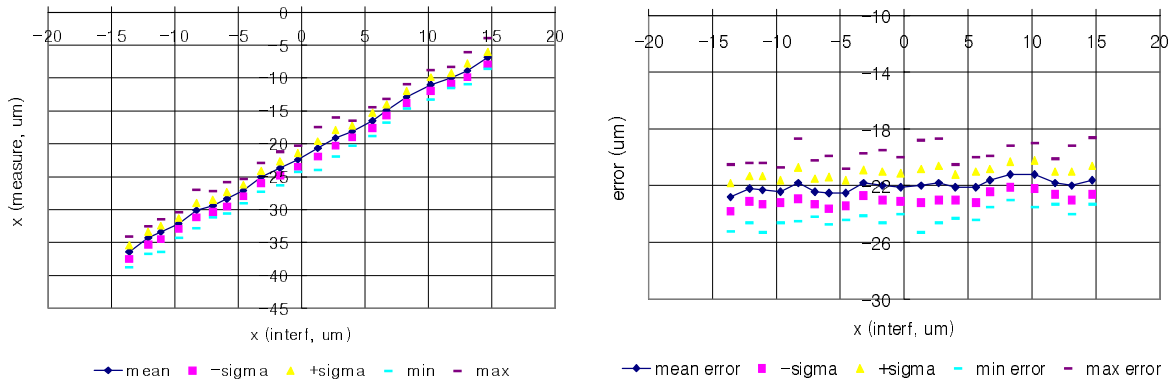

Figure 5 Measurement results of x_w-translation:
(a) Comparison between the proposed sensor readings and the interferometer readings; (b) Errors distribution

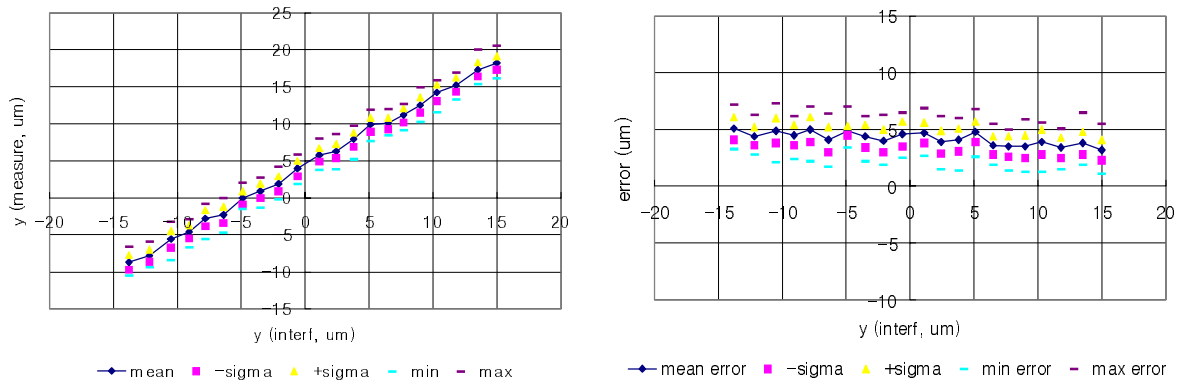

Figure 6 Measurement results in y_w-translation:
(a) Comparison between the proposed sensor readings and the interferometer readings; (b) Errors distribution

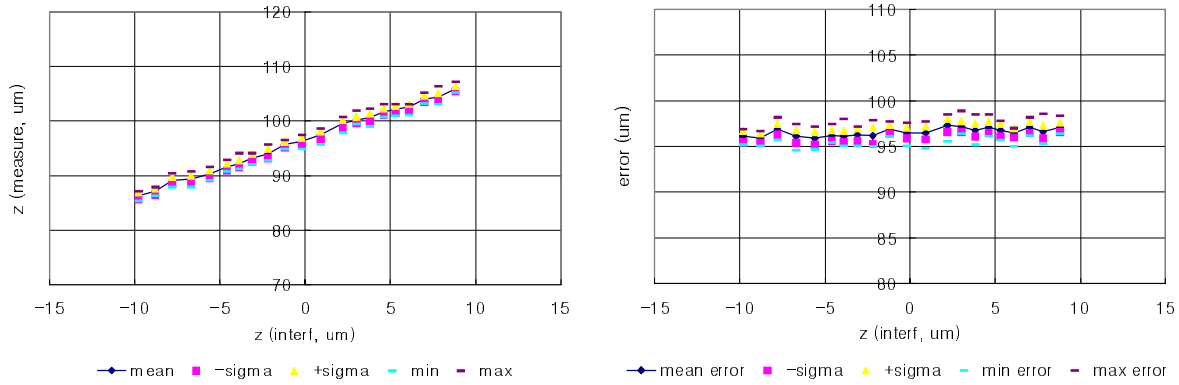

Figure 7 Measurement results in z_w-translation:
(a) Comparison between the proposed sensor readings and the interferometer readings; (b) Errors distribution

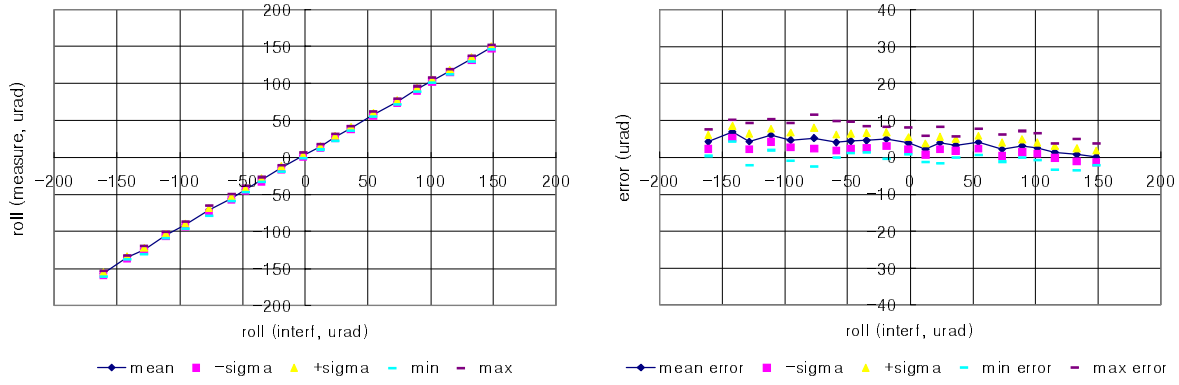

Figure 8 Measurement results in *rolling*:
(a) Comparison between the proposed sensor readings and the interferometer readings; (b) Errors distribution

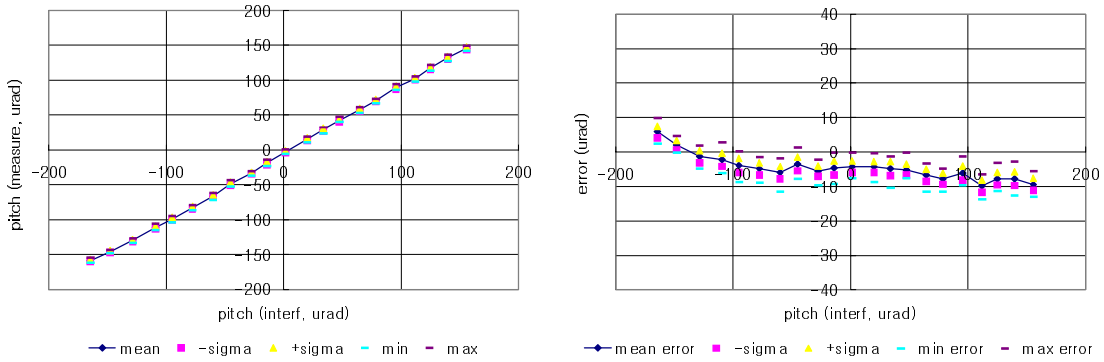

Figure 9 Measurement results in *pitching*:
(a) Comparison between the proposed sensor readings and the interferometer readings; (b) Errors distribution

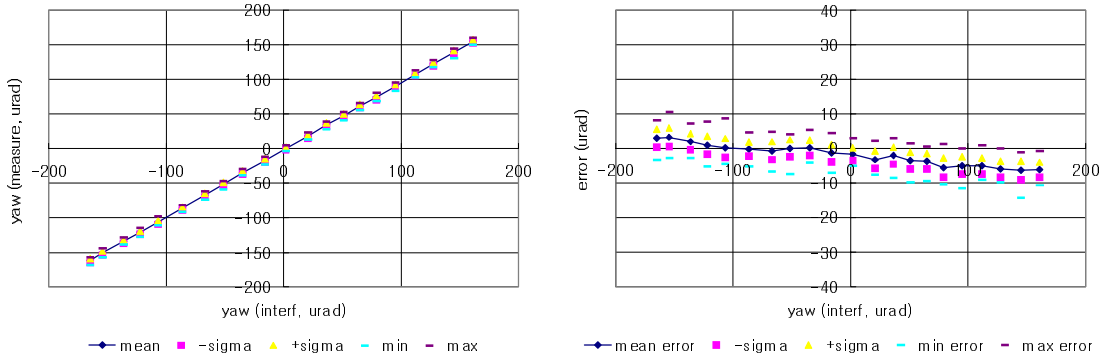

Figure 10 Measurement results in *yawing*:
(a) Comparison between the proposed sensor readings and the interferometer readings; (b) Errors distribution

In Table 2, we can see the standard deviations, each of which is the median value out of the standard deviations calculated from every data point in each axis measurement. These represent the degree of precision for the relevant axis movements in the sensor system. As shown in the table, the values are below 1μm for translations, and below 2.5 μrad for rotations. If there is a variation in the sensor reading of above two times of standard deviation in any axis, we can regard the 3-facet mirror as moving in the relevant direction with 95% probability. From this precision criterion, we can say the minimal movements in all 6-axis are 2μm for translations and 5μrad for rotations in the proposed sensor system.

Table 2 Measurement results (μm, μrad)

	Measured range	Measurement interval	Standard deviation	Relative uncertainty
x_w-translation (t_x)	28.8	1.44	0.98	11%
y_w-translation (t_y)	28.3	1.42	0.95	16%
z_w-translation (t_z)	18.6	0.93	0.63	12%
Rolling (γ)	309	15.5	1.83	2.5
Pitching (β)	310	15.5	1.80	6.1
Yawing (α)	326	16.3	2.43	4.3

4. CONCLUSION

In this paper, a new measurement system is proposed to measure the 3-dimensional positions and orientations of rigid bodies in high precision. The proposed sensor system is based on laser optics, which adopts a special mirror, 3-facet mirror, and a He-Ne laser, and three PSDs. The sensor system directly measures the 3-dimensional position and orientation of the 3-

facet mirror. And it can measure the 3-dimensional position and orientation of any object simply by mounting the 3-facet mirror on the object. In this paper, the laser light path in the system is mathematically modeled and the measurement principle is verified through a series of experiments.

The mathematical model is based on ray tracing, forward ray tracing in full, which traces the light path in the sensor system from the laser source to the destinations, three PSDs' surfaces, and yields three couples of 2-dimensional coordinates of the laser beam spots on PSDs' surfaces. On the other hand, the inversion of the forward ray tracing is performed through a numerical method. The experiments have been performed for six fundamental motions such as x, y, z-translations, and roll, pitch, yaw-rotations. In the experiments, the 3-facet mirror is moved at an extremely small interval in each axis. And both the proposed system and an interferometer measure its position and orientation, from which we can check the precision of the proposed sensor system. Through the experiments, we could verify the measurement principle is valid and the proposed sensor system can measure the movements of any object in the precision of two micrometers in translation and five micro-radians in rotation.

In the sensor model presented in this paper, the laser beam is modeled as a straight line having zero-diameter, but it somewhat differs from actual laser physics. Thus, we are to modify the model regarding the laser beam as a bundle of rays that have different intensities from each other. This is to be based on Gaussian beam optics.

ACKNOWLEDGEMENTS

This work has been performed as a part of the R&D project, Measurement of 6-DOF motion of HDD slider using a 3-facet mirror, supported by Samsung Advanced Institute of Technology, Korea.

REFERENCES

1. A. Sulzmann and J. Jacot, “3D computer vision for microassembly stations and microfabrication,” *Proc. of the SPIE*, vol. 3202, pp. 42-51, 1998.
2. X. Du and S. C. Ahalt, “3D orientation vector estimation for subcomponents of space object imagery,” *Proc. of the SPIE*, vol. 3068, pp. 395-405, 1997.
3. S. H. Or, W. S. Luk, K. H. Wong, and I. King, “An efficient iterative pose estimation algorithm,” *Proc. of the Third Asian Conference on Computer Vision*, pp. 559-566, Hong Kong, 1998.
4. S. Tachi, T. Maeda, R. Hirata, and H. Hoshino, "A construction Method of Virtual Haptic Space," *Proc. of the Fourth Int. Conf. on Artificial Reality and Tele-Existence*, pp. 131-138, Tokyo, Japan, 1994.
5. H. Yokoi, J. Yamashita, Y. Fukui, and M. Shimojo, "Development of the virtual shape manipulating system," *Proc. of the Fourth Int. Conf. on Artificial Reality and Tele-Existence*, pp. 35-42, Tokyo, Japan, 1994.
6. A. Bejczy and K. Salisbury, "Kinematic coupling between operator and remote manipulator," *Advances in Computer Technology*, vol. 1, pp. 197-211, ASME, New York.
7. J. Vaganay, M. J. Aldon, and A. Fournier, “Mobile robot attitude estimation by fusion of inertial data,” *Proc. of IEEE Conference on Robotics and Automation*, pp. 277-282, 1993.
8. K. Komoriya and E. Oyama, “Position estimation of a mobile robot using optical fiber gyroscope,” *Proc. of Intelligent Robotic Systems*, pp. 143-149, 1994.
9. B. Barshan and H. F. Durrant-Whyte, “Evaluation of a solid-state gyroscope for robotics applications,” *IEEE Trans. Instrumentation and Measurement*, vol. 44, no. 1, 1994.
10. C. A. Briggs and F. E. Talke, “The dynamics of micro sliders using laser doppler vibrometry,” *IEEE Trans. Magnetics*, vol. 26, no. 5, 1990.
11. C. A. Briggs and F. E. Talke, “Investigation of the dynamics of 50% sliders using laser doppler vibrometry,” *IEEE Trans. Magnetics*, vol. 26, no. 6, 1990.
12. T. G. Jeong and D. B. Bogy, “Slider-disk interactions during the load-unload process,” *IEEE Trans. Magnetics*, vol. 26, no. 5, pp. 2490-2492, 1990.
13. John J. Craig, *Introduction to Robotics*, Addison Wesley, 1989.
14. R. Kingslake, *Applied optics and optical engineering*, Academic Press., 1965.
15. Namir C. Shammas, *C/C++ Mathematical algorithms for scientists and engineers*, McGraw-Hill, 1996.